

CFD MODELLING AND PIV VALIDATION OF FLOW FIELD IN A FLOTATION CELL

**Jingzhong KUANG¹, Yuqing FENG^{2*}, William YANG², Peter J. WITT²,
M. Philip SCHWARZ², Tingsheng QIU¹**

¹ Jiangxi University of Science and Technology, Ganzhou 341000, CHINA

² CSIRO Mineral Resources Flagship, Clayton, Victoria 3169, AUSTRALIA

*Corresponding author, Address: Box 312, Clayton South, VIC 3169, Australia.

Email: Yuqing.Feng@csiro.au. Telephone: 61-3-95458669.

ABSTRACT

Flow characteristics in a flotation cell not only significantly affect particle suspension and froth stabilization, but also determine the flotation efficiency. This work aims to obtain a detailed understanding of the water flow in a flotation cell through combined use of single-phase Computational Fluid Dynamics (CFD) model and advanced laser measurement using Particle Image Velocimetry (PIV). The CFD model has been set up to simulate an industrial Wemco flotation cell. Following model validation using PIV measurement data at several representative planes for the same cell design and operating condition, the flow dynamics in the flotation cell have been analysed in terms of flow pattern and velocity. The results show that good agreement is achieved between predicted and measured flows with three vortices observed - one vortex below the impeller and another above the impeller, with a third small vortex found in the region near the bottom of the disperser and outside the draft tube.

Keywords: Flotation cell, CFD, PIV, flow pattern, flow dynamics

INTRODUCTION

Mineral froth flotation has been widely employed in the mineral processing industry to separate valuable minerals from gangue based on the differences in the surface hydrophobicity, and flotation machines are critical equipment in this process. Mineral flotation machines are classified into two main types: forced air and self-aerated machines.

Fluid flow characteristics are key to the successful design and operation of flotation cells. The hydrodynamics in a flotation cell not only significantly affects particle suspension and froth stability, but also controls the grade and rate of recovery and thereby determines the flotation efficiency. This has been known for many years (see for example the review by Yianatos, 2007), but Koh and Schwarz (2003, 2006) were the first to show how the performance of flotation machines could be evaluated from predictions of flow field properties such as mean velocity, turbulence level, void fraction, bubble size and bubble size distribution, by then deriving bubble-particle collision, attachment and detachment rates.

The flow dynamics in a flotation cell is very complex and still not completely characterised, particularly as several different proprietary designs are in use in industry. Computational fluid dynamics (CFD) is an effective methodology that can be used to analyse the details of the flow, as first shown by Koh et al (2000). Since then, several studies have been carried out for a variety of different cell designs, such as the Metso Minerals RCS design (Koh et al, 2003b), Outokumpu (now Outotec) design (Koh et al, 2003b, Xia et al, 2009), the Dorr-Oliver design (Salem-Said et al, 2013) and the Wemco design (Schwarz et al, 2015b, Fayed and Ragab, 2013). Both single phase (water) and two-phase (air-water) models have been described.

In most cases, the cells studied have been forced-air; eg Metso Minerals, Outotec and Dorr-Oliver cells. However, self-aerated machines have also been studied. The effect of impeller speed on the air flow in a self-aerated Denver laboratory flotation cell has been investigated using CFD (Koh and Schwarz, 2007). From two-phase simulations of the flotation cell at varying impeller speeds, the effect of increasing impeller speed was found to increase the air flow rate and gas holdup in the cell. Two-phase (water and air) flow in a self-aerated WEMCO flotation machine (0.8m³ and 300m³ models) has been investigated by Fayed and Ragab (2013) using CFD. They also devised a new boundary condition treatment, and used it in a CFD study of the transient flow structures, predicting air flow rate and power consumption as a function of time in a Wemco 0.8 m³ pilot cell (Fayed and Ragab, 2015).

Researchers have also used the CFD models to develop kinetic models of flotation rate (Koh and Schwarz, 2006, 2008). The approach is to calculate bubble-particle collision rates in different parts of the flotation cell from the local turbulent velocities, and the size and number concentrations of bubbles and particles obtained from CFD modelling (Koh, 2003a). From the collision rates, attachment and detachment rates, and the probabilities of collision, adhesion and stabilization can be calculated in each part of the cell using CFD modelling outputs (Koh, 2006). Variants of this model have been given by Karimi et al (2014a, 2014b) who provided detailed validation, and by Ragab and Fayad (2012).

CFD numerical simulation with Lagrangian particle tracking was used by Liu and Schwarz (2009a, 2009b) to improve the prediction of bubble-particle collision efficiency in a turbulent environment by concentrating on

the dynamics close to a single bubble. Such modelling was described as an example of the application of a multiscale modelling methodology for the CFD-based multiscale modelling of flotation processes (Liu and Schwarz (2009b), Schwarz et al, 2015a, 2015b).

Reliability of CFD modelling depends on validation using experimental measurement. Mavros (2001) has reviewed experimental techniques that can be used to characterize flows in stirred tanks. Particle Image Velocimetry (PIV) is a measurement technique that has been increasingly used for this purpose in the last decade. PIV gives instantaneous 2D velocity data for a whole plane in a 3D flow field. It is an ideal tool for measuring the velocity distribution in single and multiphase flow systems. Deen et al (2002a, 2002b) give details of the technique and applications to stirred vessels. The general flow pattern, velocities, and distribution of the solid and gaseous phases in a flotation apparatus were explored using a PIV system (Zachos et al, 1993).

Both LDV (laser Doppler velocimetry) and PIV have subsequently been used for validation of CFD models of flotation cells. Koh et al (2003b) detail validation using LDV data of flow velocities in various cell designs, and Tiitinen et al (2005) describe comparison of CFD predictions with LDV data taken by Zhu et al (2001) for an Outokumpu cell.

The characteristics of single phase flow field in the KYF-0.2 flotation cell were studied using CFD and PIV by Dong et al, 2013. Simulation results show that there is a vortex near the slurry-ward surface of impeller blades in the direction against the rotation direction. Furthermore, the maximum flow velocity in the flotation cell is higher than the speed at the blade tips. CFD results are in good agreement with the PIV experimental results. The single phase flow pattern of the KYF flotation cell with different impeller angles was investigated by combining PIV measurements and CFD simulation. The PIV measurement results agree with the CFD prediction results, and the backward impeller, radial impeller and forward impeller all produce similar flow patterns with upper and lower circulations. Based on the CFD simulation, the power consumption of the backward impeller is least. This result aids the structural design of impellers for KYF flotation cells (Shi, 2015).

In this paper, the single phase flow field of a Wemco flotation cell is studied using CFD simulation and PIV measurement technique.

MODEL DESCRIPTION

Geometry of flotation cell

This study was undertaken using a self-aerated Wemco flotation cell shown in Figure 1. The flotation cell consisted of a tank with an inner diameter of 1370 mm and height of 1070 mm, a draft tube with inner diameter of 305 mm, and a standpipe with inner diameter of 600 mm. The impeller has 8 blades with a diameter of 280 mm. The disperser has 48 oval holes arranged in two parallel rows. Twenty-four semi-circular rods are attached to the inner surface of the disperser. The hood consists 8 arc plates with 25 holes of diameter of 30 mm.

CFD simulations were carried out using the CFD software package ANSYS/CFX 16.0. The standard k- ϵ turbulence model was chosen, and first order upwind differencing is

used. The MRF (Multiple Reference Frames) approach is used. Convergence is based on a calculation residual less than 10^{-6} .

PIV measurement experiment

The Particle Image Velocimetry (PIV) technique is used to characterise the flow field over a plane through a physical model. For the present fluid flow structure measurements inside the flotation cell, an ILA 2D PIV system was used, consisting of a SensiCam 12-bit digital CCD camera (1280×1024 pixels), which was synchronised with a New Wave 120 mJ double-cavity Nd:YAG laser. The output laser beam, at wavelength of 532 nm, was guided through an articulated arm system to the measurement location, where the beam was expanded by a cylindrical lens to form a 1.5 to 2 mm thick planar vertical light sheet over the centre plane of the cylindrical flotation cell. The typical field of view of the CCD camera was set to $750 \times 600 \text{ mm}^2$ using 1280×1024 pixels of the CCD array. The smallest resolvable length is $586 \mu\text{m}$, which is the real length of each pixel. The interrogation windows were 64×64 pixels ($37.5 \times 37.5 \text{ mm}^2$), with 50% overlap between consecutive interrogation cells, providing a velocity vector spacing of 32 pixels (18.75 mm).

Polyamid seeding particles with a mean diameter of $50 \mu\text{m}$ and a relative density of 1.03 were used as the tracing particles for the liquid phase inside the flotation cell. It was observed that the almost neutrally buoyant polyamid particles were approximately in dynamic equilibrium with the liquid flow, therefore the particle velocity essentially equalled the local flow velocity. The relaxation time of the seeding particles is about $212 \mu\text{s}$, which is negligible compared to the laser separation time of 3 ms between the pairs of images used for computation of particle displacements. The uncertainty of pixel displacement in the measurement is about 0.2 pixels within the interrogation window of 64×64 pixels. In combination with other sources of uncertainty, such as the hardware errors of the PIV system, the laser sheet and the CCD camera misalignment, as well as the image distortion errors, it was estimated that the total PIV measurement errors of the mean velocity and its fluctuating component were approximately $\pm 2\%$ and $\pm 5\%$ respectively.

The measurements of local axial velocity by PIV were carried out at four height locations of $z = 0.90 \text{ m}$, $z = 0.71 \text{ m}$, $z = 0.53 \text{ m}$, and $z = 0.28 \text{ m}$. Figure 2 shows the four vertical location.

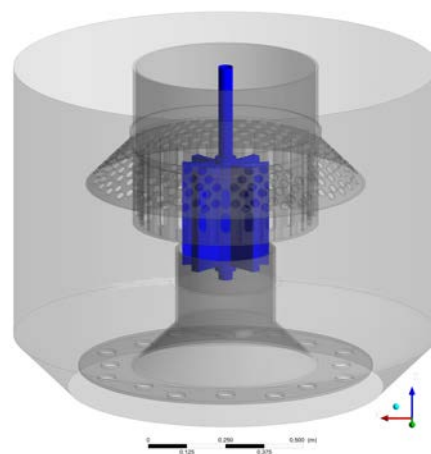


Figure1: Schematic diagram of Wemco flotation cell

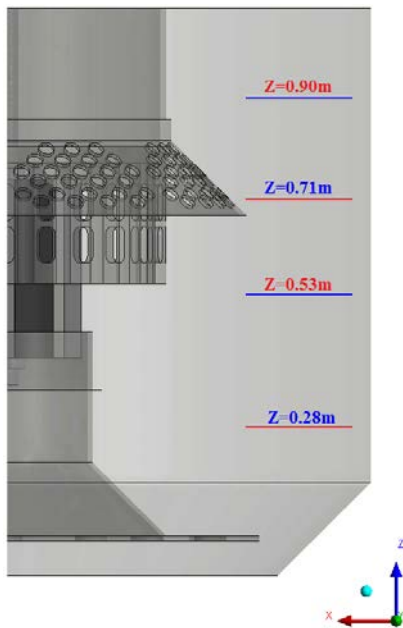


Figure 2: Four height locations for axial velocity measurement by PIV

RESULTS

Effect of mesh quality

To determine a suitable mesh, different meshes with number of nodes from 328,200 to 1,383,100 were employed to simulate the water only system at 182 rpm. Predicted streamlines in Figure 3 show that similar patterns are obtained for the three meshes, and the flow behaviour for the 639,100 and 1,383,100 node meshes are almost the same.

The axial velocity profiles at height 0.28 m are shown in Figure 4 for different meshes. Some effect of the number of mesh nodes is found: compared with the meshes with 631,900 and 1,383,100 nodes, the axial velocities for the mesh with 328,200 nodes shows differences at all radii, but predicted axial velocities for the meshes with 639,100 and 1,383,100 nodes are almost the same except close to the centre of the tank.

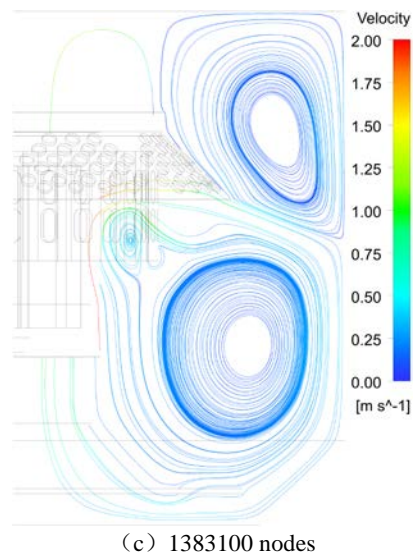
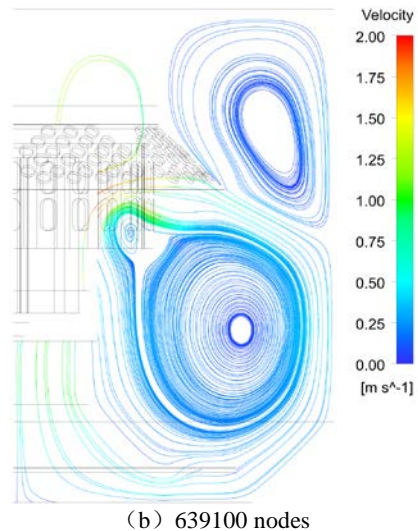
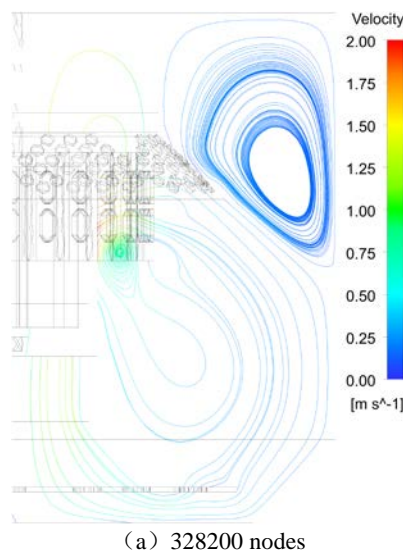


Figure 3: Comparison of streamlines predicted by CFD on the central vertical section for different meshes. Colour indicates velocity magnitude in m/s.

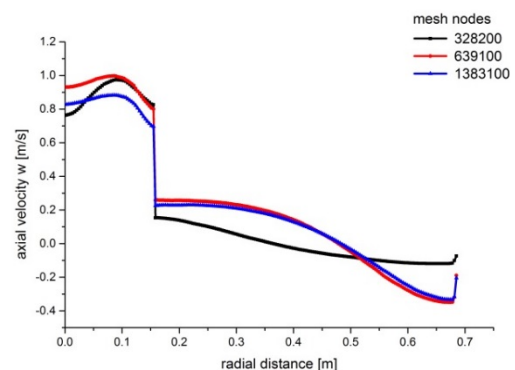


Figure 4: Axial velocity along the radial direction at height=0.28 m for three different mesh densities.

The flow rates inside the draft tube at height 0.352 m predicted by the CFD model for the three meshes are

0.0663 m³/s, 0.0598 m³/s, and 0.0602 m³/s, the flow rates for the two finest meshes being almost the same.

Thus, as a compromise between computational accuracy and computational time, the 639100 node mesh was used for all subsequent calculations.

Flow pattern comparison

The velocity vectors predicted by CFD and those obtained from measurements using the PIV technique are compared in Figure 5 on a vertical plane through the centre of the tank. Excellent agreement is achieved between predicted and measured flows with two vortices observed – one vortex below the impeller and another above the impeller. The impeller generates a jet stream in the radial direction towards the wall. The flow circulates back to the impeller through the top of the hood. This circulation vortex minimizes interaction between the upper pulp zone and the froth. The hood is designed to maintain the stability of liquid surface and froth. The lower vortex is directed towards the false bottom and through the draft tube. This circulation vortex contributes to suspension of solids and increases collisions between bubbles and solid particles. A third small vortex is found in the region near the bottom of the disperser and outside the draft tube.

Velocity comparison

Figure 6 shows profiles of CFD and PIV vertical (axial) velocity, V , along the radial direction of the tank at

various vertical locations. Predicted and measured axial velocities are in general agreement. At the top part of the tank, a maximum upward measured velocity of 0.15 m/s is found near the outer wall of the cell tank at $z = 0.90$ m, but the maximum upward CFD velocity is 0.225 m/s. Due to the anti-clockwise vortex present at the level of $z = 0.71$ m, both CFD and PIV flow fields show upflow near the wall and downflow near the hood.

The CFD and PIV vertical velocity profiles at the level $z = 0.53$ m is an inverse of that at $z = 0.71$ m, due to the large clockwise vortex there.

The height at $z = 0.53$ m intersects the lower recirculation, so there is the expected downward vertical flow near the wall at approximately $x = 0.6$ m (with maximum measured magnitude of -0.31 m/s). However, there is another downflow (maximum measured speed of 0.24 m/s), caused by the small anti-clockwise vortex underneath the disperser.

At the lower level of $z = 0.28$ m, both the CFD and PIV velocities show the profile shape typical of a recirculation outside the draft tube, $x > 0.16$ m, while inside the draft tube, a strong upward flow can be seen with the maximum velocity of 0.7 m/s (PIV) and 0.99 m/s (CFD), in the stream between the inner side of the draft tube wall and the central shaft of the impeller.

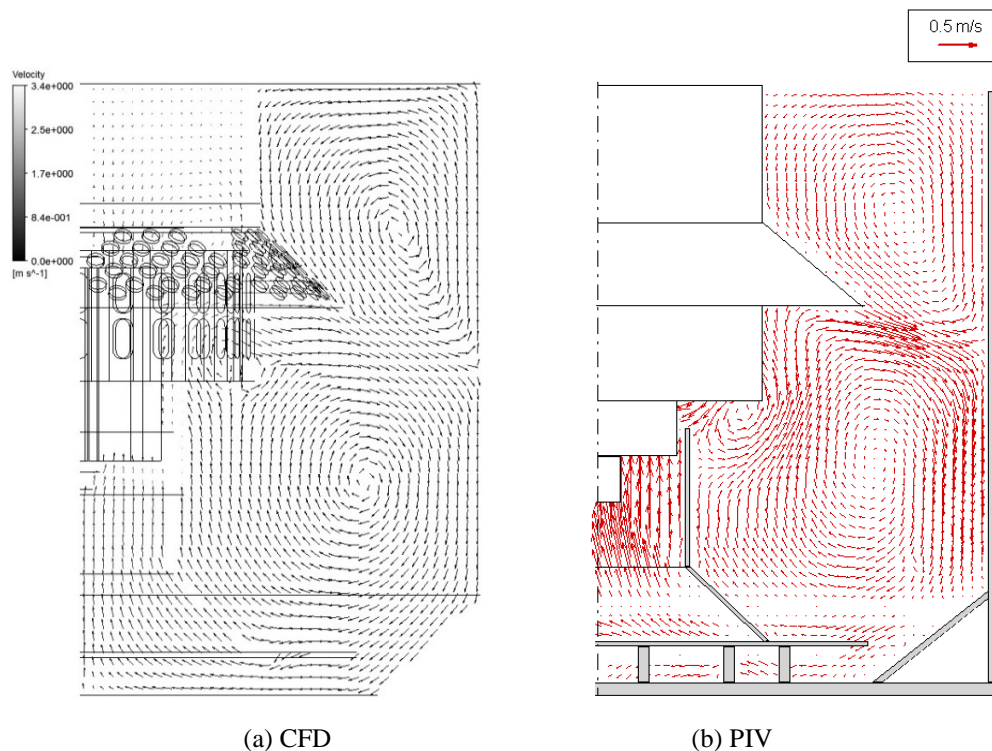


Figure 5: Comparison of CFD predicted velocity vectors with experiment measurements using PIV.

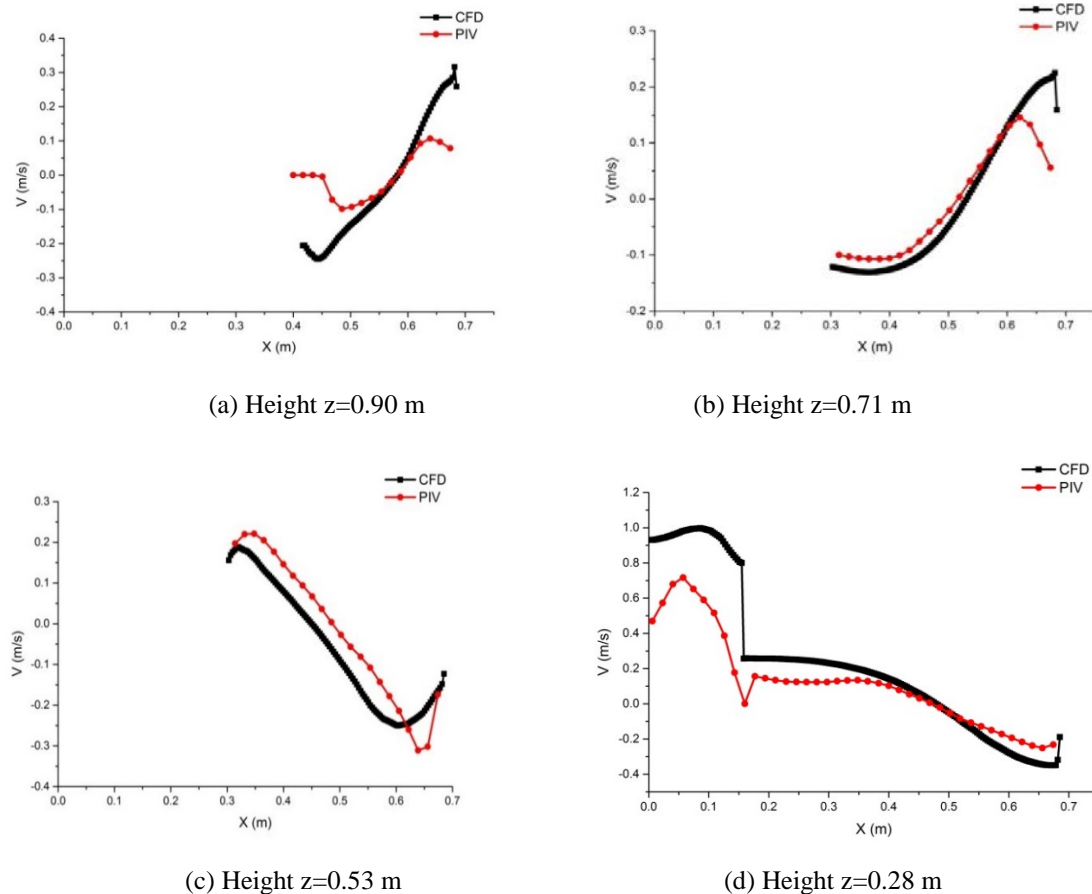


Figure 6: Comparison of predicted and measured axial velocity profiles at various vertical heights.

CONCLUSION

Good agreement is achieved between predicted and measured flow fields for the Wemco flotation cell. Both the PIV measurements and CFD modelling revealed that the rotor generated a jet stream towards the wall, which induced two strong vortices, one below the rotor level and the other extending from the rotor region to the free surface. A third small vortex is found in the region near the bottom of the disperser and outside the draft tube. The strong downward flow along the wall of the tank turns horizontally passing underneath the false bottom and up through the draft tube towards the rotor.

REFERENCES

- DEEN, N.G., WESTERWEEL, J. and DELNOIJ, E. (2002a), "Two-phase PIV in bubbly flows: Status and trends", *Chem. Eng. Technol.*, **22**, 97–101.
- DEEN, N.G., SOLBERG, T. and HJERTAGER, B.H., (2002b), "Flow generated by an aerated Rushton impeller: Two-phase PIV experiments and numerical simulations", *Canadian Journal of Chemical Engineering*, **80**, 1–15.
- DONG, G., ZHANG, M., YANG, L. and WU, F., (2013), "Analysis of flow field in the KYF flotation cell by CFD", International Conference on Process Equipment, Mechatronics Engineering and Material Science, Wuhan, China, pp. 161–165.

FAYED, H. and RAGAB S., (2013), "CFD analysis of two-phase flow in Wemco-300m³ supercell", SME/CMA Annual Meeting, February 2013, Denver, Colorado.

FAYED, H. and RAGAB S., (2015), "Numerical simulations of two-phase flow in a self-aerated flotation machine and kinetics modelling", *Minerals*, **5**, 164–188.

KARIMI, M., AKDOGAN, G. and BRADSHAW, S.M., (2014a), "A computational fluid dynamics model for the flotation rate constant, Part I: Model development", *Miner. Eng.*, **69**, 214–222.

KARIMI, M., AKDOGAN, G. and BRADSHAW, S.M., (2014b), "A CFD-kinetic model for the flotation rate constant, Part II: Model validation", *Miner. Eng.*, **69**, 203–213.

KOH, P.T.L., MANICKAM, M. and SCHWARZ, M.P., (2000), "CFD simulation of bubble-particle collisions in mineral flotation cells", *Miner. Eng.*, **13**, 1455–1463.

KOH, P.T.L. and SCHWARZ, M.P., (2003a), "CFD modelling of bubble-particle collision rates and efficiencies in a flotation cell", *Miner. Eng.*, **16**, 1055–1059.

KOH, P.T.L., SCHWARZ, M.P., ZHU Y. and BOURKE, P., (2003b), "Development of CFD models of mineral flotation cells", *Proceedings of the 3rd International Conference on CFD in the Minerals and Process Industries*, Melbourne, Australia, pp. 171–175.

KOH, P.T.L. and SCHWARZ, M.P., (2006), "CFD modelling of bubble-particle attachments in flotation cells", *Miner. Eng.*, **19**, 619–626.

KOH, P.T.L. and SCHWARZ, M.P., (2007), “CFD model of a self-aerating flotation cell”, *Int. J. Miner. Process.*, **85**, 16–24.

KOH, P.T.L. and SCHWARZ, M.P., (2008), “Modelling attachment rates of multi-sized bubbles with particles in a flotation cell”, *Miner. Eng.*, **21**, 989–993.

LIU, T.Y. and SCHWARZ, M.P., (2009a), “CFD-based modeling of bubble-particle collision efficiency with mobile bubble surface in a turbulence environment”, *Int. J. Miner. Process.*, **90**, 45–55.

LIU, T.Y. and SCHWARZ, M.P., (2009b), “CFD-based multiscale modelling of bubble-particle collision efficiency in a turbulent flotation cell”, *Chem. Eng. Sci.*, **64**, 5287–5301.

MAVROS, P., (2001), “Flow visualization in stirred vessels: A review of experimental techniques”, *Chem. Eng. Res. Des.*, **79**, 113–127.

SHI, S., ZHANG, M., FAN, X. and CHEN, D., (2015), “Experimental and computational analysis of the impeller angle in a flotation cell by PIV and CFD”, *Int. J. Min. Proc.*, **142**, 2–9.

RAGAB S., and FAYED, H., (2012), “CFD-based flotation model for prediction of pulp recovery rate”, SME Annual Meeting, February 2012, Seattle, Washington.

SALEM-SAID, A., FAYED, H. and RAGAB, S., (2013), “Numerical simulations of two-phase flow in a Dorr-Oliver flotation cell model”, *Minerals*, **3**, 284–303.

SCHWARZ, M.P., KOH, P.T.L., FENG, Y. and VERRELLI, D.I., (2015a), “Multi-scale modelling of mineral processing operations”, *Miner. Eng.*, In press.

SCHWARZ, M.P., KOH, P.T.L., VERRELLI, D.I. and FENG, Y., (2015b), “Sequential multi-scale modelling of processing operations, with application to flotation cells”, *5th International Symposium on Computational Modelling (Computational Modelling '15)*, Minerals Engineering International, June 9, 2015, Cornwall, UK.

TIITINEN, J., KOSKINEN, K. and RONKAINEN, S., (2005), “Numerical modelling of an Outokumpu flotation cell”, *Proc. Centenary of Flotation Symposium*, AusIMM., pp. 167–170.

XIA, J., RINNE, A. and GRONSTRAND, S., (2009), “Effect of turbulence models on prediction of fluid flow in an Outotec flotation cell”, *Miner. Eng.*, **22**, 880–885.

YIANATOS, J.B., (2007), “Fluid flow and kinetic modelling in flotation related processes: columns and mechanically agitated cells — a review”, *Chem. Eng. Res. Des.*, **85**, 1591–1603.

ZACHOS, A., KAISER, M. and MERZKIRCH, W., (1993), “Particle dynamics during froth flotation of hardcoal determined by means of particle image velocimetry”, *SPIE Vol. 2052*, pp. 281–288.

ZHU, Y., WU, J., SHEPHERD, I. and NGUYEN, B., (2001), CSIRO Minerals Confidential Report.